Unbiased Photoelectrode Interfaces for Solar Coupling of Lignin Oxidation with Biocatalytic C=C Bond Hydrogenation

Kim, Jinhyun; Um, Yunna; Han, Seunghyun; Hilberath, Thomas; Kim, Yong Hwan; Hollmann, Frank; Park, Chan Beum

DOI
10.1021/acsami.1c24342

Publication date
2022

Document Version
Final published version

Published in
ACS Applied Materials and Interfaces

ACS APPLIED MATERIALS & INTERFACES

www.acsami.org

Research Article

Unbiased Photoelectrode Interfaces for Solar Coupling of Lignin Oxidation with Biocatalytic C=C Bond Hydrogenation

Jinhyun Kim, Yunna Um, Seunghyun Han, Thomas Hilberath, Yong Hwan Kim, Frank Hollmann, and Chan Beum Park*

Cite This: *ACS Appl. Mater. Interfaces* 2022, 14, 11465–11473

Read Online

ACCESS | Metrics & More | Article Recommendations | Supporting Information

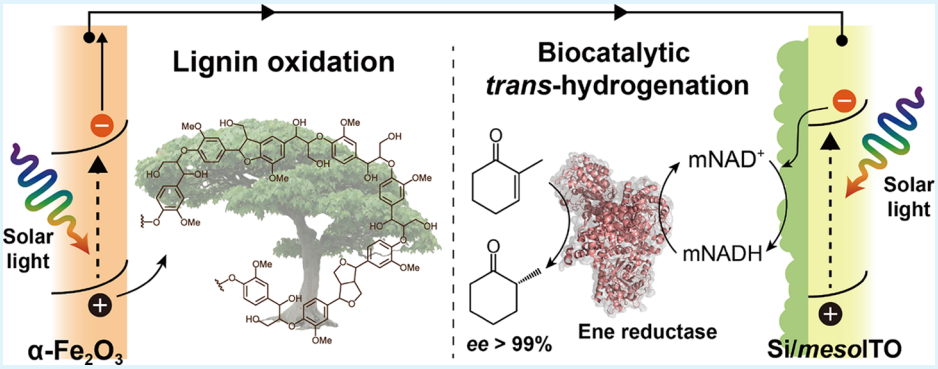

ABSTRACT: The pulp and paper manufacturers generate approximately 50 million metric tons of lignin per annum, most of which has been abandoned or incinerated because of lignin's recalcitrant nature. Here, we report bias-free photoelectrochemical (PEC) oxidation of lignin coupled with asymmetric hydrogenation of C=C bonds. The PEC platform consists of a hematite (α-Fe_2O_3) photoanode and a silicon photovoltaic-wired mesoporous indium tin oxide (Si/*meso*ITO) photocathode. We substantiate a new function of photoelectroactivated α-Fe_2O_3 to extract electrons from lignin. The extracted electrons are transferred to the Si/*meso*ITO photocathode for regenerating synthetic nicotinamide cofactor analogues (mNADHs). We demonstrate that the reduction kinetics of $mNAD^+$s depend on their reduction peak potentials. The regenerated mNADHs activate ene-reductases from the old yellow enzyme (OYE) family, which catalyze enantioselective reduction of α,β-unsaturated hydrocarbons. This lignin-fueled biocatalytic PEC system exhibits an excellent OYE's turnover frequency and total turnover number for photobiocatalytic trans-hydrogenation through cofactor regeneration. This work presents the first example of PEC regeneration of mNADHs and opens up a sustainable route for bias-free chemical synthesis using renewable lignin waste as an electron feedstock.

KEYWORDS: *lignin, hematite, photoelectrocatalysis, biocatalysis, trans-hydrogenation*

1. INTRODUCTION

Lignin is an amorphous polymer consisting of three phenylpropanoid units, accounting for approximately 10−25% of lignocellulose biomass.[1] The pulp and paper industry produces lignin with a production rate of approximately 50 million metric tons per annum.[1] However, 95% of lignin is still being abandoned or incinerated in biorefinery processes[1,2] because of its complex and irregular structure.[2] Electrocatalytic oxidation of lignin has been demonstrated using expensive catalysts under high electrical bias.[3,4] Light-driven (ideally solar-powered) oxidation routes have also been proposed.[5,6] Most photochemical lignin oxidation studies have been performed in one-pot systems using colloidal semiconductors, which generally suffer from undesirable recombination[7,8] of photo-excited charge carriers. This issue was recently addressed by ligand modification of photocatalysts,[9] which enabled efficient extraction of excitons, thereby enhancing photocatalytic activity for lignin oxidation.

Because lignin oxidation reaction is the extraction of electrons from lignin, we envisioned that coupling of lignin oxidation with valuable reductive reactions (e.g., enzymatic synthesis[10−14]) would be an appealing approach in environmental remediation and artificial photosynthesis. A photoelectrochemical (PEC) platform is a promising approach to extract electrons from lignin because of (i) broad harvesting of abundant solar energy[7] using two or more photoelectrodes and

Received: December 16, 2021
Accepted: February 2, 2022
Published: February 23, 2022

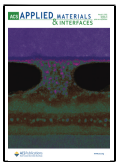

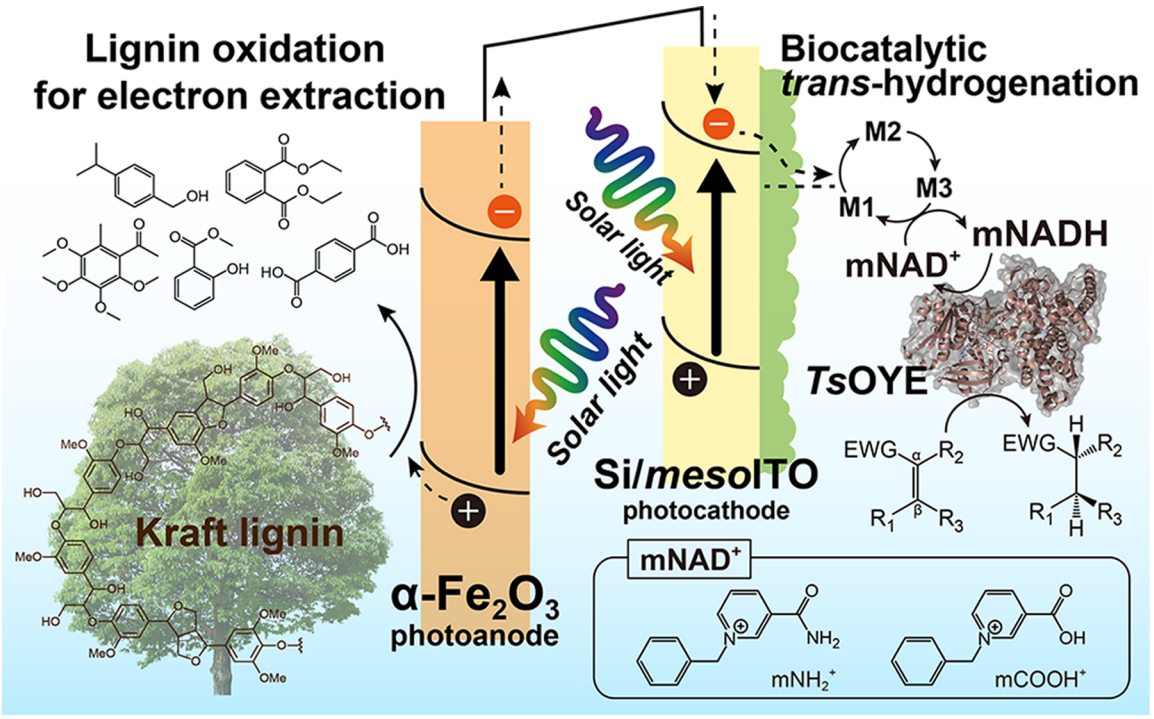

Figure 1. Illustration of a PEC platform for bias-free photoelectrocatalytic coupling of lignin oxidation and asymmetric C═C hydrogenation. The full device consists of an α-Fe_2O_3 photoanode (for lignin oxidation) and a Si/*meso*ITO photocathode (for mNADH regeneration). This PEC cell provides a large photovoltage to gain electrons from lignin, to transfer electrons to *meso*ITO, and to reduce Rh-based electron mediator (**M1**) for unbiased regeneration of (m)NADHs. These (m)NADHs transfer their hydrides to the flavin prosthetic group of the *Ts*OYE, which catalyzes trans-hydrogenation of C═C bonds. A hydride of the reduced flavin is transferred to the Cβ atom of a substrate. EWG: electron-withdrawing group. **M1**: $[Cp^*Rh(bpy)H_2O]^{2+}$. **M2**: $Cp^*Rh(bpy)$. **M3**: $[Cp^*Rh(III)(bpy)H]^+$.

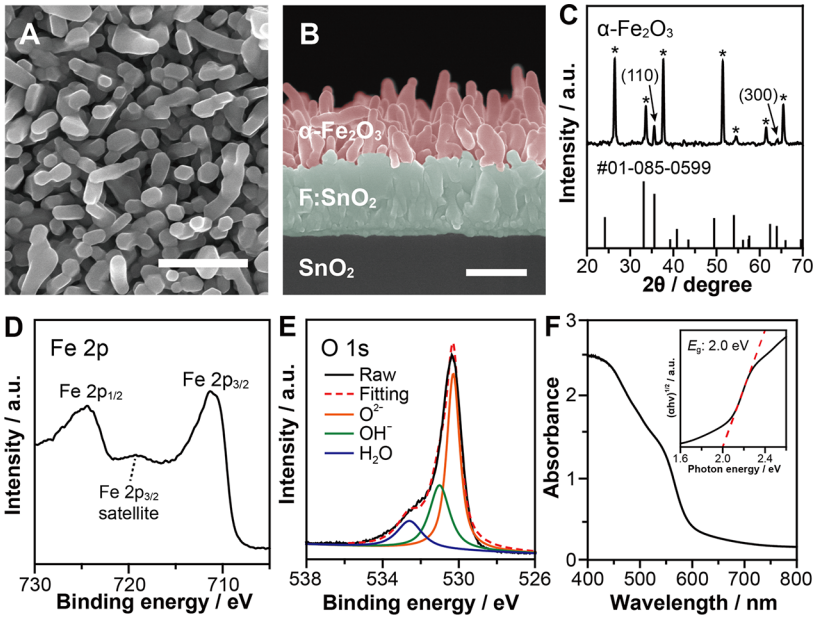

Figure 2. Characterization of the α-Fe_2O_3 electrode. (A) Plan-view scanning electron microscopy (SEM) image of the α-Fe_2O_3 electrode. Scale bar: 500 nm. (B) Cross-sectional SEM image of the photoelectrode. Scale bar: 500 nm. (C) XRD pattern of the α-Fe_2O_3 electrode. For comparison, the standard diffraction pattern of JCPDS no. #01-085-0599 is given. Asterisks denote the XRD peaks of F:SnO_2. X-ray photoelectron spectra of α-Fe_2O_3 for (D) Fe 2p and (E) O 1s. (F) Ultraviolet−visible spectrum of the α-Fe_2O_3 electrode. Inset: Tauc plot of α-Fe_2O_3 to calculate its indirect band gap, which was estimated from the intercept of tangent of the Tauc plot on the photon energy axis.

(ii) suppressed charge recombination[7] through electrical connection between photoelectrodes. In addition, PEC systems' physical separation of anodic and cathodic reaction sites enables flexible combination of redox reactions (e.g., lignin oxidation and enzymatic reaction) under different reaction conditions (e.g., electrolyte type and pH).[7]

Here, we report a bias-free PEC platform for solar-powered lignin oxidation using hematite (α-Fe_2O_3) coupled with

https://doi.org/10.1021/acsami.1c24342
ACS Appl. Mater. Interfaces 2022, 14, 11465−11473

biocatalytic asymmetric hydrogenation. As depicted in Figure 1, the PEC system consists of an α-Fe_2O_3 photoanode and a Si/mesoporous indium tin oxide (Si/*meso*ITO) photocathode. The α-Fe_2O_3 energy material takes advantage of its suitable band gap (*ca.* 2.0 eV), high PEC stability, and natural abundance.[15] We reveal a new function of α-Fe_2O_3 photoelectrodes to oxidize lignin; the photoanode transfers electrons from lignin to the Si/*meso*ITO photocathode, which we prepare by wiring an electrocatalytic *meso*ITO electrode with a Si photovoltaic (Si PV). The *meso*ITO material[16] exhibits a high electrocatalytic activity and stability in aqueous environments, whereas Si solar cells[17] are the most commercialized photovoltaics with excellent light-to-electrical power conversion efficiency and long-term stability. The photocathode produces a large photovoltage for unbiased redox reactions and reduces a Rh-based electron mediator ($[Cp^*Rh(bpy)H_2O]^{2+}$, **M1**)[7,8] for reduction of nicotinamides into the enzymatically active 1,4-dihydronicotinamides. In the present study, we choose synthetic nicotinamide analogues (mimetic NAD^+ cofactor, $mNAD^+$)[18−21]—instead of the natural cofactors—because of their tunable reactivity, economic advantages, and potentially superior stability. The reduced $mNAD^+$s (mNADHs) transfer their hydride ions to the flavin prosthetic group of old yellow enzyme homologues from *Thermus scotoductus* (*Ts*OYE).[22,23] Subsequently, the activated *Ts*OYE catalyzes the enantioselective hydrogenation of C=C bonds by delivering the hydride from the flavin N5 position to organic substrates.[18] Furthermore, lignin oxidation reaction is faster than water oxidation reaction, which is advantageous to accelerate the *Ts*OYE-driven trans-hydrogenation reaction.

2. RESULTS AND DISCUSSION

We synthesized α-Fe_2O_3 photoelectrodes through (i) formation of β-FeOOH on a F:SnO_2 (FTO) transparent conducting material and (ii) thermal phase transformation from β-FeOOH to α-Fe_2O_3. The plan-view scanning electron microscopic image of the β-FeOOH showed the formation of square nanorods (Figure S1A). We annealed the β-FeOOH electrode at 1073 K to trigger the phase transition from β-FeOOH to worm-like α-Fe_2O_3 nanostructures (Figures 2A,B and S1B). We confirmed the formation of an α-Fe_2O_3 phase using X-ray diffraction (XRD) analysis; α-Fe_2O_3's XRD pattern matched well with the reference pattern (JCPDS card number: #01-085-0599) (Figure 2C). In addition, the α-Fe_2O_3 electrode exhibited a Fe^{3+} state and a O^{2-} state on its surface (Figure 2D,E). The ultraviolet−visible absorption spectra of the α-Fe_2O_3 film displayed visible absorption, and its band gap was estimated to be approximately 2.0 eV (Figure 2F).

To investigate the capability of the α-Fe_2O_3 photoelectrode to oxidize lignin, we performed linear sweep voltammetry (LSV) analysis under simulated solar light [air mass 1.5 global (AM 1.5G), 100 mW cm^{-2}] in a three-electrode configuration. We used kraft lignin as a model lignin because it is the most available and commercialized lignin source[1] with an annual production of 130 million tons. LSV analysis—under simulated solar light (AM 1.5G, 100 mW cm^{-2}) in a three-electrode configuration—shows that anodic current densities increased with increasing lignin concentration under light conditions, but not dark conditions (Figure 3). This result indicates that (i) lignin functions as an electron donor of photoelectroactivated α-Fe_2O_3 and (ii) lignin oxidation reaction is more favorable than water oxidation reaction.

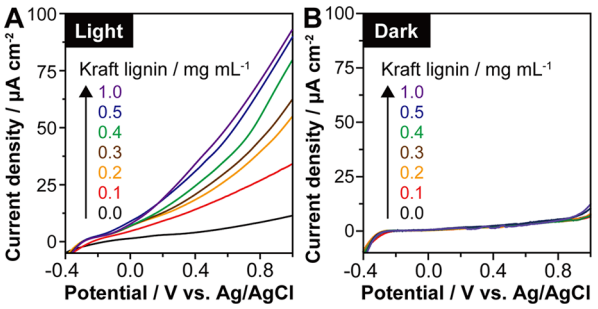

Figure 3. Photoelectrochemical analysis of α-Fe_2O_3. *J*−*V* profiles of the α-Fe_2O_3 photoanode with various lignin concentrations (0−1 mg mL^{-1}) under (A) light and (B) dark conditions. Scan rate: 50 mV s^{-1}. Electrolyte solution: a mixture of acetonitrile/deionized water (v/v = 1:1) in the absence or presence of kraft lignin. Light source: xenon lamp (AM 1.5G, 100 mW cm^{-2}). Temperature: 298 K.

We further investigated how α-Fe_2O_3 oxidized kraft lignin under four different conditions: (i) no bias under dark, (ii) anodic bias [1.0 V (vs Ag/AgCl)] under dark, (iii) no bias under solar light (AM 1.5G, 100 mW cm^{-2}), and (iv) anodic bias under solar light. In this experiment, we separated the anodic site and the cathodic site to investigate the role of α-Fe_2O_3 photoelectrodes, not a counter electrode. High-performance liquid chromatographic analysis showed a drastic oxidation of kraft lignin by approximately 60% under condition (iv) (Figure S2A; see the Supporting Information for further details on the estimation method). In contrast, the other control experiments—conditions (i), (ii), and (iii)—resulted in slight degradation less than 5%. Gel permeation chromatography analysis further supported the photoelectrocatalytic degradation of kraft lignin with α-Fe_2O_3 photoanodes; the polydispersity index of kraft lignin altered negligibly under conditions (i), (ii), and (iii) (Figure S2B). In stark contrast, the index increased by *ca.* 4.6 times under condition (iv), which suggests that photoelectroactivated α-Fe_2O_3 converts kraft lignin into oxidized fragments. The degradation reaction of kraft lignin led to the formation of aromatic molecules. As shown in Figure S3, the gas chromatography (GC)−mass spectrometric (MS) analysis result displays multiple aromatic compounds [e.g., terephthalic acid, 1-(2,3,4,5-tetramethoxy-6-methylphenyl)ethanone, methyl 2-hydroxybenzoate, (4-isopropylphenyl)methanol, and diethyl phthalate] after α-Fe_2O_3-driven photooxidation of lignin.

Because photoanodic reaction generates reactive species [e.g., holes (h^+), hydroxyl radicals ($OH^\bullet$), or hydrogen peroxides (H_2O_2)] in aqueous environments, we examined which reactive species triggered PEC lignin oxidation by supplementing a radical scavenger [e.g., Na_2SO_3 (hole scavenger) and *tert*-butyl alcohol ($OH^\bullet$ scavenger)] in the lignin solution. Note that we did not use a H_2O_2 scavenger because our assay using 2,2′-azino-bis-(3-ethylbenzothiazoline-6-sulfonic acid)[24] confirmed negligible formation of H_2O_2 with the α-Fe_2O_3 photoanode. As shown in Figure S2C, the addition of the hole scavenger led to a considerable decrease in lignin photodegradation, whereas the $OH^\bullet$ scavenger showed a slight effect on lignin oxidation. This result indicates that α-Fe_2O_3's photoexcited holes play an important role in the PEC degradation of lignin. We obtained additional evidence of the participation of photoexcited holes in the lignin oxidation reactions using Fourier-transform infrared (FT-IR) spectroscopic analysis. Photoexcited holes have been reported to

https://doi.org/10.1021/acsami.1c24342
ACS Appl. Mater. Interfaces 2022, 14, 11465−11473

oxidize C_α–OH to C_α=O at C_α position of lignin.[5,6,25] As shown in Figure S2D, an absorbance band at *ca.* 1726 cm^{-1}, which corresponds to C=O bond stretching,[26] increased after the photoanodic reaction.

Photocatalytic and electrocatalytic oxidation reactions of lignin have been reported[1,2] to depolymerize lignin through various oxidative routes. Among them, we hypothesized that α-Fe_2O_3 can drive oxidative cleavage of β-aryl ether (β-O-4)—the most frequent linkage in lignin[2,27]—because (i) our FT-IR result shows an increase in the number of C=O functional groups of kraft lignin (Figure S2D) and (ii) the oxidation of C_α–OH to C_α=O is a key step[1,5,6,25] in oxidative dissociation of lignin's β-O-4 linkage. To verify the hypothesis, we selected guaiacylglycerol-β-guaiacyl ether as a model lignin dimer that contains a β-O-4 bond. In accordance with the results obtained with kraft lignin, we observed that α-Fe_2O_3's photocurrent density increased with increasing concentrations of the dimer (Figure S4). In addition, the photoactivated α-Fe_2O_3 yielded guaiacol from the model compound under anodic bias (Figure S5), which we attribute to (i) oxidation of C_α–OH to C_α=O and (ii) subsequent oxidation of C_α–C_β on the basis of the oxidative pathway[1] of lignin depolymerization.

As a cathode that receives electrons from α-Fe_2O_3-driven lignin oxidation, we synthesized a *meso*ITO material by drop-casting ITO suspension on a FTO substrate and annealing it at 673 K. As displayed in Figure S6A, the as-synthesized *meso*ITO exhibited mesoporous morphology with a pore diameter of 50 nm. The *meso*ITO's XRD pattern matched with the cubic ITO's pattern (JCPDS card number: #01-083-3350), implying that no composition change occurred during the film formation (Figure S6B). Because a higher electrochemically active surface area (ECSA) of a conductive electrode is advantageous for augmenting the rate of redox reactions,[16] we increased *meso*ITO's ECSA by tuning the amount of ITO suspension cast on the FTO substrate. To estimate the relative ECSA, we estimated *meso*ITO's double-layer capacitance (C_{dl}) because C_{dl} is linearly proportional to the ECSA[28,29] of a conducting material with similar composition. We found that the C_{dl} of *meso*ITO increased from 0 to 6.63 mF cm^{-2} as the amount of ITO suspension increased from 0 to 20 μL (Figure S6C,D). This result indicates that *meso*ITO electrode provides a higher ECSA than planar ITO electrode.

We connected the *meso*ITO cathode with a Si PV in series to build a single photocathode that generates sufficient photovoltage for bias-free regeneration of (m)NADHs. The assembly of the *meso*ITO cathode and the Si PV (Si/*meso*ITO) resulted in an anodic shift of 3 V in the J–V profile of the *meso*ITO (Figure S7), which we attribute to the provision of Si's photovoltage for the *meso*ITO electrode. We found that the Si PV increased the *meso*ITO's cathodic current; as shown in the photocurrent density profiles (Figure S8), Si/*meso*ITO showed a higher cathodic current than *meso*ITO under solar light (AM 1.5G and 100 mW cm^{-2}) at 2.1 V (vs Ag/AgCl). We ascribe the result to more negative potential of electrons driven by the photoactivated Si solar cell. In addition, the photocathodic current of Si/*meso*ITO was higher than that of Si/ITO due to *meso*ITO's higher ECSA than ITO's ECSA. Overall, these results suggest that the Si/*meso*ITO assembly can function as a photocathode for bias-free PEC regeneration of mNADHs.

Our LSV analysis verified the reduction of **M1** with the Si/*meso*ITO photocathode. Note that (photo)electrocatalysts reduce **M1** to $[Cp^*Rh(bpy)H]^+$ (**M3**) via $Cp^*Rh(bpy)$ (**M2**),[7,8,30,31] and **M3** regiospecifically reduces (m)NAD^+ to enzymatically active 1,4-(m)NADH.[18,19] The J–V curve from the *meso*ITO film showed a generation of photocathodic current when we supplemented **M1** into an electrolyte solution (Figure 4A), which indicates the reduction of **M1** on the surface of the *meso*ITO film. In addition, the cathodic current further increased with the addition of 1-benzyl-3-carbamoyl-pyridinium ions (mNH_2^+) (Figure 4A), which we attribute to the consecutive transfer of photoexcited electrons from *meso*ITO to mNH_2^+ via **M**. We estimated the rate of mNH_2H regeneration under different conditions at 2.1 V (vs Ag/AgCl). As shown in Figure S9, planar ITO and *meso*ITO cathodes did not regenerate mNH_2H in the absence of any key components (e.g., light or Si PV). Under illumination, the mNH_2H regeneration rate of Si/*meso*ITO was much higher than that of Si/planar ITO, which we attribute to the higher ECSA of *meso*ITO than planar ITO.

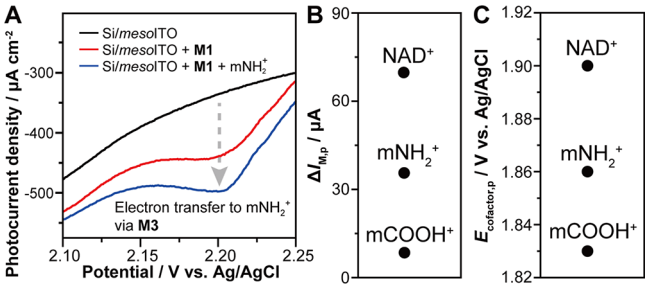

Figure 4. Photoelectrochemical analysis of cofactor reduction driven by the Si/*meso*ITO photocathode. (A) Changes in LSVs of the Si/*meso*ITO photocathode with the sequential addition of redox compounds (i.e., **M1** and mNH_2^+). Scan rate: 50 mV s^{-1}. (B) Comparison of changes in the cathodic peak current of 0.5 mM **M1** in the presence of 1 mM cofactor at 2.2 V (vs Ag/AgCl). (C) Reduction peak potentials of cofactors. Solvent in (A–C): TEOA-buffered solution (100 mM, pH 7.5). Light intensity in (A–C): 1 sun.

We further investigated the regeneration of different types of cofactors [e.g., 1,4-dihydronicotinamide adenine dinucleotide (NADH), 1-benzyl-1,4-dihydropyridine-3-carboxamide (mNH_2H), and 1-benzyl-1,4-dihydropyridine-3-carboxylic acid (mCOOHH)] using the Si/*meso*ITO photocathode. The reduction rate of $mNAD^+$s to mNADHs was in the order of NADH > mNH_2H > mCOOHH (Figure S10). This tendency was consistent with the degree of **M** mediation in the reduction of the cofactors measured by the increase in the reduction peak current of **M1** as shown in Figures 4B and S11. We attribute the result to different reduction peak potentials ($E_{cofactor,p}$) in the order of NAD^+ > mNH_2^+ > $mCOOH^+$ (Figures 4C and S12) because **M1**'s driving force[19] for cofactor reduction becomes higher as $E_{cofactor,p}$ gets more positive.

Building on the results, we paired the α-Fe_2O_3 photoanode with the Si/*meso*ITO photocathode to drive unbiased reduction of NAD analogues using lignin as electron feedstocks. We predicted a bias-free redox reaction with α-Fe_2O_3/Si/*meso*ITO with an expected operation current of 227 μA according to the overlaying $|I|$–V plots of the photoelectrodes (Figure 5A). To increase the operation current, we increased the geometric surface area of the α-Fe_2O_3 electrode for boosting the rate of cofactor regeneration. As shown in Figure 5B, the increase in α-Fe_2O_3's geometrical surface area from 1 to 4 cm^2 resulted in (i) a higher saturated photocurrent by lignin oxidation and (ii) a larger expected operation current

https://doi.org/10.1021/acsami.1c24342
ACS Appl. Mater. Interfaces 2022, 14, 11465–11473

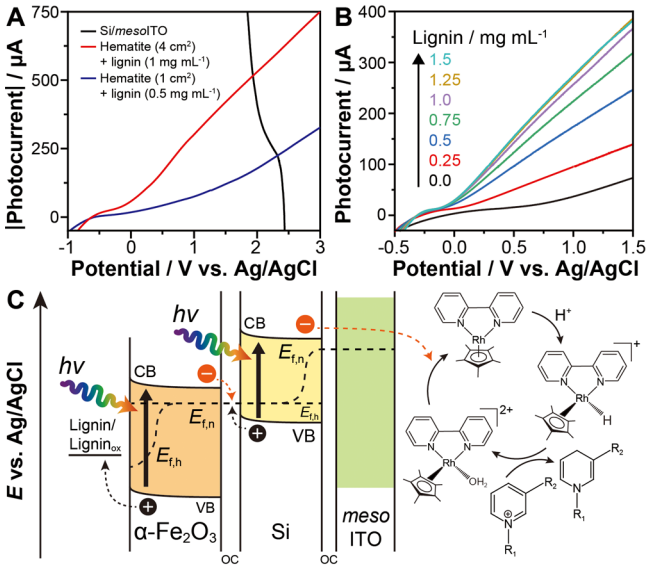

Figure 5. Unbiased regeneration of (m)NADHs driven by the α-Fe_2O_3/Si/*meso*ITO photoelectrocatalytic system. (A) Overlaps of $|I|-V$ profiles of different-sized α-Fe_2O_3 photoanodes and a Si/*meso*ITO photocathode. (B) LSV of a 4 cm^2 hematite photoelectrode with various concentrations of kraft lignin (0−1.5 mg mL^{-1}) under solar light (1 sun). Scan rate: 50 mV s^{-1}. Temperature: 298 K. (C) Plausible mechanism of unbiased mNADH regeneration fueled by lignin. OC: Ohmic contact. CB: conduction band. VB: valence band. $E_{f,n}$: quasi-Fermi level of electrons. $E_{f,h}$: quasi-Fermi level of holes. R_1: CH_2Ph (mNH_2^+ and $mCOOH^+$). R_2: $CONH_2$ (mNH_2^+) or COOH ($mCOOH^+$).

(474 μA; Figure 5A). The unbiased PEC system regenerated mNH_2H from mNH_2^+ using solar light as a sole energy resource, and the mNH_2H regeneration rate increased with lignin concentration from 0 to 1 mg mL^{-1} (Figure S13). The unbiased regeneration rate of mNADHs was in the order of NADH > mNH_2H > mCOOHH (Figure S14). Control experiments in the absence of light or Si PV resulted in a negligible regeneration of (m)NADHs (Figure S14), which indicates that the provision of Si's photovoltage for the PEC system is a key for driving bias-free regeneration of cofactors.

We propose the pathway of photoinduced transfer of electrons from lignin to (m)NAD^+ based on the widely accepted mechanism[16,32] of photoelectrochemistry (Figure 5C). Solar light absorption by dual absorbers (i.e., α-Fe_2O_3 and Si) generates photoexcited charge carriers. The α-Fe_2O_3 photoanode transfers its photoexcited holes to lignin, while α-Fe_2O_3's photoexcited electrons are recombined with the Si's photoexcited holes. The energy levels of Si's excited electrons are negative enough to reduce **M1** on the surface of *meso*ITO. In terms of quasi-Fermi levels (E_f), light absorption by photoelectrodes redistributes minority carriers with corresponding electrons' E_f ($E_{f,n}$) and holes' E_f ($E_{f,h}$). Under solar light, the $E_{f,h}$ of α-Fe_2O_3 becomes more positive than lignin's oxidation potential, which drives the transfer of photoexcited holes from α-Fe_2O_3 to lignin. Likewise, the $E_{f,n}$ of *meso*ITO is more negative than reduction potential of **M1**, which makes electrons migrate from *meso*ITO to **M1**.

Counting on solar-powered regeneration of mNH_2H using kraft lignin as a major electron source, we further applied the regeneration of mNADHs to *Ts*OYE-catalyzed trans-hydro-

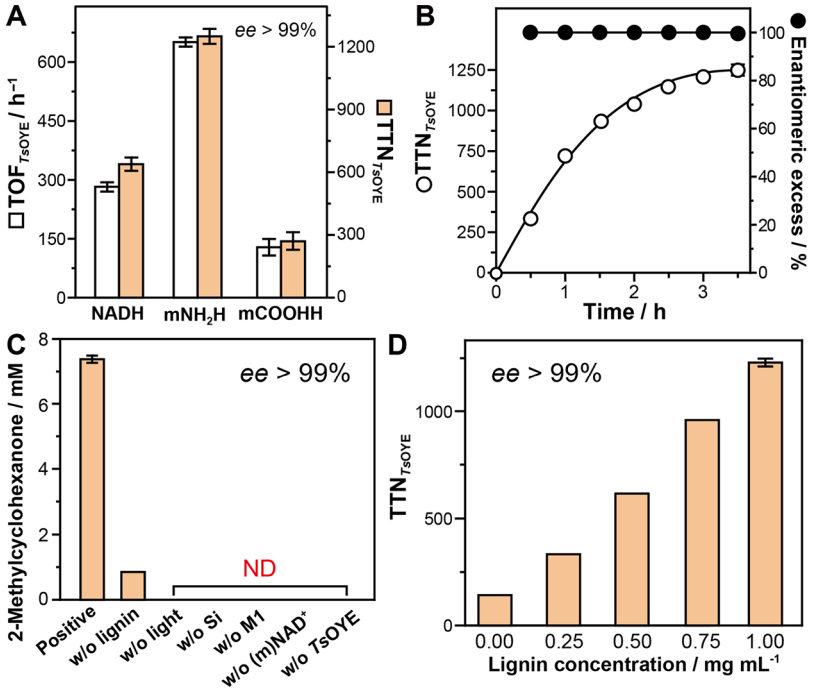

Figure 6. Bias-free biocatalytic asymmetric hydrogenation of C=C bonds. (A) *Ts*OYE's turnover frequency (TOF_{TsOYE}) and the total turnover number (TTN_{TsOYE}) for photoelectrocatalytic reduction of 2-methyl-2-cyclohexen-1-one under solar light. TOF_{TsOYE} and TTN_{TsOYE} were determined after 30 and 210 min, respectively. (B) Time profiles of TTN_{TsOYE} and enantiomeric excess (ee) for unbiased biocatalytic conversion of 2-methyl-2-cyclohexen-1-one. (C) Control experiments of bias-free biocatalytic PEC hydrogenation of C=C bonds. The reaction condition of the positive group was the same as that in panel (A). (D) Effect of lignin concentration on TTN_{TsOYE}. Cathodic electrolyte solution in (A−D): TEOA-buffered solution (100 mM, pH 7.5) containing **M1**, cofactor, $MgSO_4$, *Ts*OYE, and 2-methyl-2-cyclohexen-1-one. Kraft lignin concentration in (A−C): 1 mg mL^{-1}. Light intensity in (A−D): 1 sun. Temperature in (A−D): 298 K. Error bars correspond to the standard deviation (n = 3). ND: not detected.

https://doi.org/10.1021/acsami.1c24342
ACS Appl. Mater. Interfaces 2022, 14, 11465−11473

Table 1. Comparison of Efficiencies of State-of-the-Art PEC Systems that Regenerate Cofactors for *Ts*OYE-Driven Reduction of α,β-Unsaturated Compounds

photoelectrocatalyst	electrical bias [V]	regenerated cofactor type	TOF_{OYE} [h^{-1}]	TTN_{OYE}	reference
α-Fe_2O_3/Si/*meso*ITO	0	mNH_2H	650 ± 20	1250 ± 40	this study
Mo:$BiVO_4$/IO-ITO	0.5−1.0	FMN_{red}[a]	50	110[b]	29
FeOOH/$BiVO_4$/CNT/C_3N_4	0.3−0.9	FMN_{red}[a]	130	260[b]	33

[a]Reduced form of flavin mononucleotide. [b]Approximate estimation based on data from the corresponding reference.

genation of conjugated C═C bonds. The exposure of the α-Fe_2O_3/Si/*meso*ITO PEC system to solar light drove unbiased reduction of 2-methyl-2-cyclohexen-1-one to enantiopure (*R*)-2-methylcyclohexanone [enantiomeric excess (ee) > 99%] with different production yields (in the order of mNH_2H > NADH > mCOOHH) (Figure 6A,B). The order of the enzymatic production rate was not identical to that of the cofactor regeneration rate, which we ascribe to better kinetic parameters of mNH_2H; according to the literature,[18] mNH_2H exhibits a higher specificity constant for the *Ts*OYE (533 mM^{-1} s^{-1}) than NADH does (163 mM^{-1} s^{-1}). The omission of solar light or Si PV from the biocatalytic PEC system did not drive asymmetric hydrogenation of C═C bonds (Figure 6C), which we attribute to imperceptible formation of (m)NADHs (Figure S14). In addition, both photosynthetic components [i.e., **M1**, (m)NAD^+, and *Ts*OYE] and organic substrates were requisites for asymmetric hydrogenation of C═C bonds (Figure 6C). We also observed that photobiocatalytic performance increased with increasing lignin concentration (Figure 6D), indicating that the α-Fe_2O_3 photoanode consumes lignin as an electron feedstock to drive photoinduced electron transfer to the *Ts*OYE. When we used 1 mg mL^{-1} lignin and 6 μM *Ts*OYE, mNH_2H regeneration exhibited the highest *Ts*OYE's turnover frequency of 650 ± 20 h^{-1} and the highest *Ts*OYE's total turnover number of 1250 ± 40 among three different cofactors (Figure 6A). These values are much higher compared with other reports[29,33] on the combination of the *Ts*OYE and photoelectrocatalysts under applied electrical bias (Table 1).

Overall, this study demonstrates that α-Fe_2O_3 extracts electrons from lignin wastes for driving enantioselective hydrogenation reactions with excellent performances. We envision that the PEC regeneration of mNADHs can be further applied to activate various redox enzymes[19,34] (e.g., cytochrome P450, enoate reductase, monooxygenase, D-lactate dehydrogenase, malic enzyme, and malate dehydrogenase) for solar-to-chemical conversion. Future challenges for attaining higher photobiocatalytic efficiencies would be (i) photoanode's doping or morphological/dimensional change to increase hole concentrations at the semiconductor−electrolyte interface, (ii) investigation of α-Fe_2O_3's active sites for lignin oxidation and augmentation of the active sites to boost the lignin oxidation reaction, (iii) functionalization of the cathode with graphitic carbon materials[35] to accelerate charge transfer to **M1**, and (iv) modification of mediator's redox potential to enhance (m)NADH regeneration performance.

3. CONCLUSIONS

We designed a α-Fe_2O_3/Si/*meso*ITO PEC system for bias-free coupling of lignin oxidation and biocatalytic trans-hydrogenation of C═C bonds. This work demonstrates for the first time (i) the capability of α-Fe_2O_3 energy material to oxidize lignin under solar light and (ii) the photoelectrocatalytic regeneration of mNADHs. Our mechanistic studies reveal that the oxidation half-reaction occurs *via* transfer of photoexcited holes from the photoanode to lignin substrates, which results in (i) oxidation of hydroxyl to carbonyl groups and (ii) oxidative cleavage of lignins' β-O-4 bonds. Concurrently, the photoanode extracts electrons from lignin and delivers the electrons to the Si/*meso*ITO photocathode for mNADH regeneration and redox biotransformation. We elucidate the capability of the porous *meso*ITO to reduce **M1** for highly regioselective regeneration of (m)NADH cofactors. Lignin-fueled regeneration of mNADHs triggers *Ts*OYE-catalyzed synthesis of enantiopure (*R*)-2-methylcyclohexanone (ee > 99%). Compared with other cofactors, the unbiased PEC regeneration of mNH_2H exhibits the best performance (TOF_{TsOYE}: 650 ± 20 h^{-1} and TTN_{TsOYE}: 1250 ± 40), which we attribute to the mNH_2H's higher specificity constant for the *Ts*OYE. Furthermore, these turnover numbers are much higher in photobiocatalytic trans-hydrogenation through cofactor regeneration. Overall, lignin-fueled regeneration of better-than-nature cofactor analogues is a renewable and sustainable approach for efficient biocatalytic photosynthesis using lignin waste and solar light.

4. EXPERIMENTAL METHODS

4.1. Chemicals. Iron(III) chloride hexahydrate, sodium nitrate, indium tin oxide nanopowder, acetic acid, ethanol, sodium sulfite, acetonitrile, oxidized nicotinamide adenine dinucleotide, kraft lignin, and acetone were purchased from Sigma-Aldrich (St. Louis, MO, USA). These chemicals were used without further purification. Artificial nicotinamide analogues, the OYE from *T. scotoductus* (*Ts*OYE), and $[Cp^*Rh(bpy)H_2O]^{2+}$ (designated anion: Cl^-) were prepared according to the literature.[19,30] We used type 1 ultrapure water (18 MΩ cm) from a Direct-Q 5 UV ultrapure water purification system (Millipore Corp., USA).

4.2. Fabrication of Hematite, *meso*ITO, and Photovoltaic/Cathode Electrodes. We prepared a hematite photoanode via solution-based processing and high-temperature annealing. A commercial F:SnO_2 (FTO) glass (TEC-7, Pilkington) was purchased and washed with acetone, ethanol, and deionized water. To deposit a β-FeOOH film on the FTO substrate, we prepared a solution containing 0.15 M $FeCl_3 \cdot 6H_2O$ and 1 M $NaNO_3$ in deionized water, immersed the FTO substrate in the solution, and heated it in a furnace (Fisher Scientific Co., USA) at 100 °C for 6 h. To transform β-FeOOH into α-Fe_2O_3, we annealed the electrode at 800 °C for 20 min. A *meso*ITO electrode was synthesized according to the literature.[16] We prepared an ITO suspension by adding 40 mg of ITO nanoparticles (<50 nm in diameter) in 193 μL of an acetic acid/ethanol (300:748 v/v) mixture. We ultrasonicated the suspension for 120 min and homogenized it for 30 min. We drop-cast 20 μL of the ITO suspension on a FTO substrate (surface area: 1 cm^2). Subsequently, the electrode was annealed at 400 °C for 1 h. According to the literature,[16] the active area of the *meso*ITO can be controlled by changing the surface area of the FTO. We purchased a planar ITO glass (Taewon Scientific Corp, Korea) as a control group. A Si/*meso*ITO photocathode was prepared by wiring a *meso*ITO cathode to a commercial Si solar cell (YOLK). The electron-collecting contact area of the Si photovoltaic was wired to the FTO side of the *meso*ITO electrode using Cu tape. The hole-collecting contact area of

https://doi.org/10.1021/acsami.1c24342
ACS Appl. Mater. Interfaces 2022, 14, 11465−11473

the Si solar cell was also attached using Cu tape for further wiring with the FTO side of the photoanode. The ratio of the geometrical surface areas of α-Fe_2O_3, Si, and *meso*ITO can be tuned under the condition that the light size is large enough to activate the entire area of the photoelectrodes (i.e., α-Fe_2O_3 and Si).

4.3. PEC Oxidation of Lignin. We used a potentiostat/galvanostat (WMPG 1000, WonATech Co., Korea) and a 450 W xenon lamp (Newport Co., USA) to conduct the photoelectrochemistry. We constructed a one-compartment, three-electrode configuration consisting of a working electrode (α-Fe_2O_3), a reference electrode (Ag/AgCl and 3 M NaCl), and a counter electrode (Pt wire). When we adopted a two-compartment fashion, the counter electrode was located in the other chamber; the two chambers were connected using a salt bridge, which maintained electrical neutrality. To prepare electrolyte solutions, we dissolved kraft lignin in a mixture of acetonitrile and deionized water (v/v = 1:1). The light intensity was 1 sun, which we measured using an ILT 1400-A radiometer (International Light Technologies Co., USA). Because kraft lignin absorbed ultraviolet and visible light, we brought the α-Fe_2O_3's glass substrate into contact with the surface of the reactor so that incident light passes through α-Fe_2O_3 first. We used a 1260 Infinity liquid chromatography system (Agilent Technologies, USA) to estimate the degree of lignin oxidation. The conditions of high-performance liquid chromatography (HPLC) were as follows: injection, 0.02 mL; mobile phase, acetonitrile/deionized water (v/v: 6/4); flow rate, 0.6 mL min^{-1}; column, Inertsil ODS-3V; temperature: 35 °C; detector, variable wavelength detector; and wavelength, 280 nm. The lignin oxidation was estimated according to eq 1

$$\text{lignin oxidation (\%)} = \frac{I_{t=0} - I_t}{I_{t=0}} \times 100 \quad (1)$$

where I is the integration of the HPLC signal of lignin and t is the PEC reaction time. The solubility of kraft lignin in 60% acetonitrile aqueous solution was gravimetrically determined to be 73.9 ± 2.0 g L^{-1} (n = 5). To estimate its solubility, we added kraft lignin (80 mg) in the solution (1 mL), magnetically stirred the lignin solution for 24 h, and obtained insoluble residues using vacuum filtration at room temperature. Subsequently, the residues were vacuum-dried at 323 K for 6 h, and their mass was measured using a microbalance. For gel permeation chromatography analysis, we acetylated the lyophilized lignin sample (10 mg) using a mixture of pyridine (0.5 mL) and acetic anhydride (0.5 mL) at 323 K. We obtained an acetylated sample by (i) 10-fold dilution with water, (ii) centrifugation, and (iii) drying it under a vacuum at 308 K. We dissolved the acetylated sample in tetrahydrofuran (4 mg mL^{-1}) and filtered it using a polytetrafluoroethylene membrane filter with a pore size of 200 nm. Polydispersity indexes were measured using an Agilent 1200S system equipped with an Optilab rEX (RI) detector. The eluent was tetrahydrofuran with a flow rate of 1.0 mL min^{-1}. We used a Nicolet iS50 FTIR spectrometer (Thermo Scientific Inc., USA) to obtain Fourier-transform infrared spectra of lignin samples. We analyzed oxidation products using GC−MS. The oxidation products were extracted using dichloromethane and injected into a DB-5 MS column (60 m × 250 μm × 0.25 μm). The oven temperature was elevated from 323 to 553 K. The product's mass spectrum was identified using an authentic library of standards. The mass analyzer range was 5−1050 amu (scan time: 0.2 s) with positive ion polarity.

4.4. PEC Regeneration of Synthetic Nicotinamide Analogues. We performed photoelectrocatalytic regeneration of (m)NADH in a one-compartment, three-electrode configuration, which consisted of a 1 cm^2 *meso*ITO (working electrode), an Ag/AgCl (reference electrode), and a Pt wire (counter electrode). We prepared an electrolyte solution by dissolving $[Cp^*Rh(bpy)H_2O]^{2+}$ (**M1**) and (m)NAD^+ in a triethanolamine (TEOA) buffer (100 mM, pH 7.5) for mNADH regeneration. We monitored the concentration of the mNADH using a V-650 UV−vis absorption spectrophotometer (JASCO Inc., Japan); the absorption peak position and the molar extinction coefficient of NADH, mNH_2H, and mCOOHH were 340 nm and 6220 M^{-1} cm^{-1}, 360 nm and 7254 M^{-1} cm^{-1}, and 283 nm and 8988 M^{-1} cm^{-1}, respectively.[19]

4.5. Bias-Free Biocatalytic PEC Reactions Fueled by Lignin. We coupled lignin oxidation reaction with cofactor regeneration reaction in two different reactors, which were connected by a salt bridge. We dissolved kraft lignin in a mixture of acetonitrile and deionized water (v/v = 1:1) and immersed the photoanode in the solution. We prepared a cathodic electrolyte solution [0.5 mM **M1** and 1 mM cofactor in a TEOA-buffered solution (100 mM, pH 7.5)], and immersed a *meso*ITO electrode in the solution; the TEOA solution was placed in a disposable cuvette, through which light cannot penetrate. A Si photovoltaic was placed in front of the disposable cuvette and connected to the *meso*ITO cathode. Subsequently, we constructed a two-electrode configuration by connecting the α-Fe_2O_3 photoanode and the Si/*meso*ITO photocathode. The geometrical surface areas of α-Fe_2O_3, *meso*ITO, and Si photovoltaic were 4, 1, and 0.96 cm^2, respectively. The photoanode and the solar cell were irradiated with solar light using a xenon lamp (Newport Co., USA, 1 sun). For lignin-fueled biocatalytic PEC reduction of C=C bonds, unless otherwise specified, the cathode's electrolyte solution was a TEOA-buffered solution (100 mM and pH 7.5) containing 1 mM **M1**, 1 mM cofactor, 25 mM $MgSO_4$, 6 μM *Ts*OYE, and 9 mM 2-methyl-2-cyclohexen-1-one and photoanode's electrolyte was a mixture of deionized water and acetonitrile containing 1 mg mL^{-1} kraft lignin. We quantified the product using GC (Agilent Technologies Inc., USA). The TOF_{TsOYE} and TTN_{TsOYE} were calculated according to the following equations [eqs 2 and 3]

$$\text{TOF}_{TsOYE}\ (h^{-1}) = \frac{\text{[product] at a given time}}{[TsOYE] \times \text{time}} \quad (2)$$

$$\text{TTN}_{TsOYE} = \frac{\text{maximum [product] at a given time}}{[TsOYE]} \quad (3)$$

■ ASSOCIATED CONTENT

Supporting Information

The Supporting Information is available free of charge at https://pubs.acs.org/doi/10.1021/acsami.1c24342.

Characterization of β-FeOOH and *meso*ITO electrodes, GC−MS analysis, FT-IR analysis, PEC analyses, and comparison of performance of cofactor regeneration (PDF)

■ AUTHOR INFORMATION

Corresponding Author

Chan Beum Park − *Department of Materials Science and Engineering, Korea Advanced Institute of Science and Technology (KAIST), Daejeon 305-701, Republic of Korea;* orcid.org/0000-0002-0767-8629; Email: parkcb@kaist.ac.kr

Authors

Jinhyun Kim − *Department of Materials Science and Engineering, Korea Advanced Institute of Science and Technology (KAIST), Daejeon 305-701, Republic of Korea;* orcid.org/0000-0002-1616-1891

Yunna Um − *Department of Materials Science and Engineering, Korea Advanced Institute of Science and Technology (KAIST), Daejeon 305-701, Republic of Korea*

Seunghyun Han − *School of Energy and Chemical Engineering, Ulsan National Institute of Science and Technology (UNIST), Ulsan 44919, Republic of Korea;* orcid.org/0000-0003-1557-2178

Thomas Hilberath − *Department of Biotechnology, Delft University of Technology, Delft 2629HZ, The Netherlands;* orcid.org/0000-0002-9778-2509

Yong Hwan Kim − *School of Energy and Chemical Engineering, Ulsan National Institute of Science and Technology (UNIST), Ulsan 44919, Republic of Korea*
Frank Hollmann − *Department of Biotechnology, Delft University of Technology, Delft 2629HZ, The Netherlands;* orcid.org/0000-0003-4821-756X

Complete contact information is available at: https://pubs.acs.org/10.1021/acsami.1c24342

Author Contributions

J.K. conceived and designed the research. C.B.P. supervised the research. J.K. and Y.U. performed (photo)electrochemical experiments and analyzed the results. S.H. and Y.H.K. discussed and analyzed lignin oxidation. F.H. and T.H. prepared unspecific peroxygenases. F.H. discussed the enzymatic reaction. J.K., Y.U., and C.B.P. co-wrote the article. J.K. revised the article.

Notes

The authors declare no competing financial interest.

■ ACKNOWLEDGMENTS

This work was supported by the National Research Foundation (NRF) (grant nos. NRF-2015R1A3A2066191 and 2017M1A2A2087630) and the Global Ph.D. Fellowship Program (grant no. NRF-2019H1A2A1075810), Republic of Korea.

■ REFERENCES

(1) Wang, M.; Wang, F. Catalytic Scissoring of Lignin into Aryl Monomers. *Adv. Mater.* **2019**, *31*, 1901866.
(2) Li, C.; Zhao, X.; Wang, A.; Huber, G. W.; Zhang, T. Catalytic Transformation of Lignin for the Production of Chemicals and Fuels. *Chem. Rev.* **2015**, *115*, 11559−11624.
(3) Cai, P.; Fan, H.; Cao, S.; Qi, J.; Zhang, S.; Li, G. Electrochemical Conversion of Corn Stover Lignin to Biomass-based Chemicals between Cu/NiMoCo Cathode and Pb/PbO_2 Anode in Alkali Solution. *Electrochim. Acta* **2018**, *264*, 128−139.
(4) Shao, D.; Liang, J.; Cui, X.; Xu, H.; Yan, W. Electrochemical Oxidation of Lignin by Two Typical Electrodes: Ti/$SbSnO_2$ and Ti/PbO_2. *Chem. Eng. J.* **2014**, *244*, 288−295.
(5) Liu, H.; Li, H.; Lu, J.; Zeng, S.; Wang, M.; Luo, N.; Xu, S.; Wang, F. Photocatalytic Cleavage of C−C Bond in Lignin Models under Visible Light on Mesoporous Graphitic Carbon Nitride through $\pi-\pi$ Stacking Interaction. *ACS Catal.* **2018**, *8*, 4761−4771.
(6) Han, G.; Yan, T.; Zhang, W.; Zhang, Y. C.; Lee, D. Y.; Cao, Z.; Sun, Y. Highly Selective Photocatalytic Valorization of Lignin Model Compounds Using Ultrathin Metal/CdS. *ACS Catal.* **2019**, *9*, 11341−11349.
(7) Kim, J.; Park, C. B. Shedding Light on Biocatalysis: Photoelectrochemical Platforms for Solar-driven Biotransformation. *Curr. Opin. Chem. Biol.* **2019**, *49*, 122−129.
(8) Lee, S. H.; Choi, D. S.; Kuk, S. K.; Park, C. B. Photobiocatalysis: Activating Redox Enzymes by Direct or Indirect Transfer of Photoinduced Electrons. *Angew. Chem., Int. Ed.* **2018**, *57*, 7958−7985.
(9) Wu, X.; Xie, S.; Liu, C.; Zhou, C.; Lin, J.; Kang, J.; Zhang, Q.; Wang, Z.; Wang, Y. Ligand-Controlled Photocatalysis of CdS Quantum Dots for Lignin Valorization under Visible Light. *ACS Catal.* **2019**, *9*, 8443−8451.
(10) Son, G.; Kim, J.; Park, C. B. Interference of Solvatochromic Twist in Amyloid Nanostructure for Light-Driven Biocatalysis. *ACS Appl. Energy Mater.* **2020**, *3*, 1215−1221.
(11) Wang, D.; Kim, J.; Park, C. B. Lignin-Induced $CaCO_3$ Vaterite Structure for Biocatalytic Artificial Photosynthesis. *ACS Appl. Mater. Interfaces* **2021**, *13*, 58522−58531.
(12) Hobisch, M.; Schie, M. M. C. H.; Kim, J.; Røjkjær Andersen, K.; Alcalde, M.; Kourist, R.; Park, C. B.; Hollmann, F.; Kara, S. Solvent-Free Photobiocatalytic Hydroxylation of Cyclohexane. *ChemCatChem* **2020**, *12*, 4009−4013.
(13) Choi, D. S.; Lee, H.; Tieves, F.; Lee, Y. W.; Son, E. J.; Zhang, W.; Shin, B.; Hollmann, F.; Park, C. B. Bias-Free In Situ H_2O_2 Generation in a Photovoltaic-Photoelectrochemical Tandem Cell for Biocatalytic Oxyfunctionalization. *ACS Catal.* **2019**, *9*, 10562−10566.
(14) Kuk, S. K.; Ham, Y.; Gopinath, K.; Boonmongkolras, P.; Lee, Y.; Lee, Y. W.; Kondaveeti, S.; Ahn, C.; Shin, B.; Lee, J. K.; Jeon, S.; Park, C. B. Continuous 3D Titanium Nitride Nanoshell Structure for Solar-Driven Unbiased Biocatalytic CO_2 Reduction. *Adv. Energy Mater.* **2019**, *9*, 1900029.
(15) Iandolo, B.; Wickman, B.; Zorić, I.; Hellman, A. The Rise of Hematite: Origin and Strategies to Reduce the High Onset Potential for the Oxygen Evolution Reaction. *J. Mater. Chem. A* **2015**, *3*, 16896−16912.
(16) Kim, J.; Lee, Y. W.; Choi, E.-G.; Boonmongkolras, P.; Jeon, B. W.; Lee, H.; Kim, S. T.; Kuk, S. K.; Kim, Y. H.; Shin, B.; Park, C. B. Robust FeOOH/$BiVO_4$/Cu(In, Ga)Se_2 Tandem Structure for Solar-powered Biocatalytic CO_2 Reduction. *J. Mater. Chem. A* **2020**, *8*, 8496−8502.
(17) Battaglia, C.; Cuevas, A.; De Wolf, S. High-efficiency Crystalline Silicon Solar Cells: Status and Perspectives. *Energy Environ. Sci.* **2016**, *9*, 1552−1576.
(18) Knaus, T.; Paul, C. E.; Levy, C. W.; de Vries, S.; Mutti, F. G.; Hollmann, F.; Scrutton, N. S. Better than Nature: Nicotinamide Biomimetics That Outperform Natural Coenzymes. *J. Am. Chem. Soc.* **2016**, *138*, 1033−1039.
(19) Kim, J.; Lee, S. H.; Tieves, F.; Choi, D. S.; Hollmann, F.; Paul, C. E.; Park, C. B. Biocatalytic C=C Bond Reduction through Carbon Nanodot-Sensitized Regeneration of NADH Analogues. *Angew. Chem., Int. Ed.* **2018**, *57*, 13825−13828.
(20) Paul, C. E.; Arends, I. W. C. E.; Hollmann, F. Is Simpler Better? Synthetic Nicotinamide Cofactor Analogues for Redox Chemistry. *ACS Catal.* **2014**, *4*, 788−797.
(21) Guarneri, A.; van Berkel, W. J.; Paul, C. E. Alternative Coenzymes for Biocatalysis. *Curr. Opin. Biotechnol.* **2019**, *60*, 63−71.
(22) Opperman, D. J.; Piater, L. A.; van Heerden, E. A Novel Chromate Reductase from Thermus scotoductus SA-01 Related to Old Yellow Enzyme. *J. Bacteriol.* **2008**, *190*, 3076−3082.
(23) Kim, J.; Lee, S. H.; Tieves, F.; Paul, C. E.; Hollmann, F.; Park, C. B. Nicotinamide Adenine Dinucleotide as a Photocatalyst. *Sci. Adv.* **2019**, *5*, No. eaax0501.
(24) Yoon, J.; Kim, J.; Tieves, F.; Zhang, W.; Alcalde, M.; Hollmann, F.; Park, C. B. Piezobiocatalysis: Ultrasound-Driven Enzymatic Oxyfunctionalization of C−H Bonds. *ACS Catal.* **2020**, *10*, 5236−5242.
(25) Yoo, H.; Lee, M.-W.; Lee, S.; Lee, J.; Cho, S.; Lee, H.; Cha, H. G.; Kim, H. S. Enhancing Photocatalytic β-O-4 Bond Cleavage in Lignin Model Compounds by Silver-Exchanged Cadmium Sulfide. *ACS Catal.* **2020**, *10*, 8465−8475.
(26) Shao, L.; Zhang, X.; Chen, F.; Xu, F. Fast Pyrolysis of Kraft Lignins Fractionated by Ultrafiltration. *J. Anal. Appl. Pyrolysis* **2017**, *128*, 27−34.
(27) Wang, D.; Lee, S. H.; Kim, J.; Park, C. B. "Waste to Wealth": Lignin as a Renewable Building Block for Energy Harvesting/Storage and Environmental Remediation. *ChemSusChem* **2020**, *13*, 2807−2827.
(28) Su, J.; Yang, Y.; Xia, G.; Chen, J.; Jiang, P.; Chen, Q. Ruthenium-cobalt Nanoalloys Encapsulated in Nitrogen-doped Graphene as Active Electrocatalysts for Producing Hydrogen in Alkaline Media. *Nat. Commun.* **2017**, *8*, 14969.
(29) Choi, D. S.; Kim, J.; Hollmann, F.; Park, C. B. Solar-Assisted eBiorefinery: Photoelectrochemical Pairing of Oxyfunctionalization and Hydrogenation Reactions. *Angew. Chem., Int. Ed.* **2020**, *59*, 15886−15890.
(30) Lee, Y. W.; Boonmongkolras, P.; Son, E. J.; Kim, J.; Lee, S. H.; Kuk, S. K.; Ko, J. W.; Shin, B.; Park, C. B. Unbiased Biocatalytic Solar-

to-Chemical Conversion by FeOOH/$BiVO_4$/perovskite Tandem Structure. *Nat. Commun.* **2018**, *9*, 4208.
(31) Hollmann, F.; Witholt, B.; Schmid, A. $[Cp^*Rh(bpy)(H_2O)]^{2+}$: a Versatile Tool for Efficient and Non-enzymatic Regeneration of Nicotinamide and Flavin Coenzymes. *J. Mol. Catal. B: Enzym.* **2002**, *19*−*20*, 167−176.
(32) Kuk, S. K.; Jang, J.; Kim, J.; Lee, Y.; Kim, Y. S.; Koo, B.; Lee, Y. W.; Ko, J. W.; Shin, B.; Lee, J. K.; Park, C. B. CO_2-Reductive, Copper Oxide-Based Photobiocathode for Z-Scheme Semi-Artificial Leaf Structure. *ChemSusChem* **2020**, *13*, 2940−2944.
(33) Son, E. J.; Lee, S. H.; Kuk, S. K.; Pesic, M.; Choi, D. S.; Ko, J. W.; Kim, K.; Hollmann, F.; Park, C. B. Carbon Nanotube−Graphitic Carbon Nitride Hybrid Films for Flavoenzyme-Catalyzed Photoelectrochemical Cells. *Adv. Funct. Mater.* **2018**, *28*, 1705232.
(34) Le, T. K.; Kim, J.; Anh Nguyen, N.; Huong Ha Nguyen, T.; Sun, E. G.; Yee, S. M.; Kang, H. S.; Yeom, S. J.; Beum Park, C.; Yun, C. H. Solar-Powered Whole-Cell P450 Catalytic Platform for C-Hydroxylation Reactions. *ChemSusChem* **2021**, *14*, 3054−3058.
(35) Lee, J. S.; Lee, S. H.; Kim, J.; Park, C. B. Graphene−Rh-complex Hydrogels for Boosting Redox Biocatalysis. *J. Mater. Chem. A* **2013**, *1*, 1040−1044.

https://doi.org/10.1021/acsami.1c24342
ACS Appl. Mater. Interfaces 2022, 14, 11465−11473